RSC Advances

PAPER

View Article Online
View Journal | View Issue

Cite this: *RSC Adv.*, 2020, **10**, 9786

The synthesis of a DHAD/ZnAlTi-LDH composite with advanced UV blocking and antibacterial activity for skin protection†

Xinlong Liu,[a] Tingting Hu,[b] Guishan Lin,[a] Xiu Wang,[a] Yu Zhu,[b] Ruizheng Liang,[*b] Wengui Duan*[a] and Min Wei[b]

Received 19th January 2020
Accepted 27th February 2020

DOI: 10.1039/d0ra00572j

rsc.li/rsc-advances

Skin wounds are particularly vulnerable and susceptible to bacterial infection. Unfortunately, the abuse of antibiotics has resulted in the emergence of a number of multidrug-resistant bacteria in the past few decades. Moreover, secondary damage of the fragile new tissue around the wound caused by high-energy ultraviolet (UV) radiation has been rarely noticed. To address these problems, herein, we present an alternative strategy to overcome drug-resistant bacteria and UV damage by taking advantage of dehydroabietic acid derivatives (DHADs) and layered double hydroxides (LDHs). DHAD, synthesized from dehydroabietic acid (DHA) through a series of reactions, was assembled with ZnAlTi-LDH to obtain a DHAD/ZnAlTi-LDH composite. The results showed that DHAD/ZnAlTi-LDH has a prominent reactive oxygen species (ROS) production capacity, and both Gram-negative and positive bacteria can be killed under visible light irradiation. At the same time, it can effectively shield the skin from UV rays. *In vitro* and *vivo* experiments confirmed that the composite has great promise for bactericidal applications, UV blocking and wound healing.

Introduction

Skin is the largest organ of the human body with a lot of prominent functions, such as protection, excretion, temperature regulation and feeling of external stimuli.[1] However, as the first line of defense in direct contact with the outside world, the skin is so sensitive that it can easily be damaged. Skin damage is often accompanied by a bacterial infection that will threaten human health.[2] Many severe diseases, for instance, septic arthritis and dermatosis, are caused by bacterial infection when the skin gets injured.[3] As a result, how to accelerate the healing of skin wounds has become an urgent need for human health. Antibiotics such as vancomycin are capable of killing different kinds of bacteria, and therefore are hailed as one of the most significant advances for public health and life.[4] Unfortunately, antibiotics are often abused in clinical treatment, which has resulted in the emergence of a number of multi-resistant bacteria that are harmful to humans.[5] Thus, alternative methods that can inhibit these multi-resistant bacteria are highly needed.[6] What's more, bacterial infection is not the only cause that blocks the healing of skin wounds; UV-induced injury is also a large obstacle. The new tissue around the wound is very fragile and therefore can easily be damaged again by high-energy UV rays in comparison to normal skin.[7] In consequence, in order to accelerate wound healing, antibacterial treatment and UV protection must be taken into consideration simultaneously.

Antibacterial photocatalytic therapy (APCT), an alternative solution to traditional antibiotics, has been reported in recent years.[8] Different from traditional antibiotics, APCT employs photocatalysts to split water and oxygen to generate a myriad of reactive oxygen species (ROS), such as hydroxyl radicals ($^{\cdot}OH$) and singlet oxygen ($^1O_2$), which can react with the protein, lipid, polysaccharide of bacteria membrane and lead to bacterial perforation and death.[9] Previous works commonly utilized metal-based photocatalysts, such as CdS/TiO_2, WO_3/TiO_2, $BiVO_4/WO_3$,[10,11] however, heavy metal species in the photocatalysts would induce the risk of toxicity, which limited their further application.[12] The fabrication of organic–inorganic composite without heavy metal irons is a promising method, however, it has been rarely studied for antibacterial and wound healing.[13,14]

Layered double hydroxides (LDHs), with the formula expressed as $[M_{1-x}^{2+}M_x^{3+}(OH)_2](A^{n-})_{x/n}\cdot mH_2O$, is made up of positively charged metal host layers and exchangeable interlayer anions.[15] Our previous works indicated LDH possesses low toxicity and superior biocompatibility and its unique 2D structure makes it an excellent drug carrier.[16] Dehydroabietic acid

[a]School of Chemistry and Chemical Engineering, Guangxi University, Nanning 530004, Guangxi, China. E-mail: wgduan@gxu.edu.cn

[b]State Key Laboratory of Chemical Resource Engineering, Beijing Advanced Innovation Center for Soft Matter Science and Engineering, Beijing University of Chemical Technology, Beijing 100029, P. R. China. E-mail: liangrz@mail.buct.edu.cn

† Electronic supplementary information (ESI) available. See DOI: 10.1039/d0ra00572j

(DHA) is a valuable forestry resource with antibacterial activity.[17,18] According to its structure, it has multiple modification sites such as carboxyl group and benzene ring. A wide range of biological activities, such as insecticidal, antimicrobial, anticancer and anti-inflammatory, had been reported from dehydroabietic acid derivatives (DHAD).[19,20] However, the application of DHA and its derivatives is greatly limited by their poor water solubility. Herein, an ultrathin 2D composite was fabricated by loading DHAD onto ZnAlTi-LDH nanosheets, which possesses excellent antibacterial and UV resistance performance. A new DHAD was synthesized from DHA through a series of reactions, with intrinsic antibacterial activity and UV absorption property. At the same time, ZnAlTi-LDH nanosheets with a thickness of ~1.1 nm and a lateral size of ~60 nm were synthesized with good morphology and crystallinity. The DHAD/ZnAlTi-LDH composite possesses excellent capacity to produce $^{\cdot}OH$ and $^1O_2$ as well as UV resistance performance. *In vitro* tests verified a superior antibacterial efficacy of DHAD/ZnAlTi-LDH with a bacteria growth inhibition rate of 94% (*E. coli*) and 91% (*S. aureus*) respectively under visible light irradiation. *In vivo* experiments showed that DHAD/ZnAlTi-LDH promoted wound healing and reduced the skin damage caused by UV radiation synergistically, which shows the potential applications in antibacterial treatment and UV protection.

Results and discussion

As one of the benzophenone-like UV-absorbers, DHAD is synthesized from DHA through a series of reactions as showed in Scheme 1A. Its structure was characterized by ^{1}H-NMR, ^{13}C-NMR, Fourier transform infrared (FT-IR) and electrospray ionization-mass (ESI-MS) spectrometry (ESI, S1–S12†). UV-vis absorption spectra showed that the UV absorption intensity of DHAD at 200–320 nm is much stronger than that of DHA (Fig. 1A). Then, ZnAlTi-LDH with different Al^{3+} incorporation ratios were synthesized by a "bottom-up" method.[21] The XRD patterns were shown in Fig. 1B. There were some impurity phases in the ZnTi-LDH sample. The sharp and strong (003) and (006) reflections enhanced gradually when the ratio of Al^{3+} increased, and $Zn_{2.0}Al_{0.2}Ti_{0.8}$-LDH and $Zn_{2.0}Al_{0.3}Ti_{0.7}$-LDH indicated a typical LDH phase with good crystallinity. Moreover, the UV absorption indicated that $Zn_{2.0}Al_{0.2}Ti_{0.8}$-LDH possesses the optimal absorption at the UV region (Fig. S13†). Taking into account of the crystallization and UV absorption, $Zn_{2.0}Al_{0.2}Ti_{0.8}$-LDH was chosen for the following study ($Zn_{2.0}Al_{0.2}Ti_{0.8}$-LDH was replaced by LDH or ZnAlTi-LDH unless specified). The transmission electron microscope (TEM) image of ZnAlTi-LDH displayed a plate-like morphology with a lateral dimension of ~60 nm (Fig. 1C). And high-resolution TEM (HRTEM) image of ZnAlTi-LDH with a lattice spacing of 0.178 nm was assigned to (110) lattice plane. AFM image indicated a sheet-like structure with a thickness of ~1.1 nm (Fig. 1D). Moreover, the hydrodynamic diameter of ZnAlTi-LDH is measured for 86.2 ± 5.2 nm in three different mediums (water, PBS, DMEM) and without any sensible changes in particle sizes within 7 days (Fig. S14†). X-ray photoelectron spectroscopy (XPS) was performed to explore the chemical composition and valence state of ZnAlTi-LDH (Fig. S15†). Peaks at 1021.9 and 1044.7 eV were assigned to Zn^{2+} $2p_{3/2}$ and $2p_{1/2}$, peak at 74.3 eV was attributed to Al^{3+} 2p, and peaks at 458.5 and 464.3 eV corresponded to Ti^{4+} $2p_{3/2}$ and $2p_{1/2}$. The chemical compositions determined by inductively coupled plasma atomic emission spectroscopy (ICP-AES) were listed in Table S1,† which is mainly consistent with the feed ratio.

The loading performance of ZnAlTi-LDH toward DHAD was studied. The loading content (LC) and encapsulation efficiency

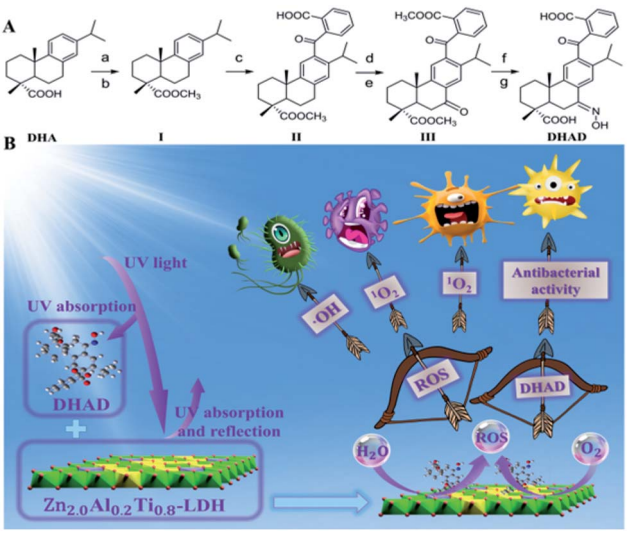

Scheme 1 (A) Synthetic pathway to targeted compounds and (B) a schematic illustration for DHAD/LDH toward advanced UV blocking and antibacterial activity. Reagents and conditions: (a) benzene, $SOCl_2$, 80 °C, 3 h. (b) CH_3OH, 80 °C, 3 h. (c) *o*-Phthalic anhydride, DCM, $AlCl_3$, rt, 6 h. (d) Benzene, $SOCl_2$, 80 °C, 3 h. Then, CH_3OH, 80 °C, 3 h. (e) CrO_3, CH_3COOH, 80 °C. 9 h. (f) Hydroxylamine hydrochloride, CH_3-CH_2OH, Et_3N, 80 °C, 8 h. (c) $KOBu^t$, DMSO, 70 °C, 5 h.

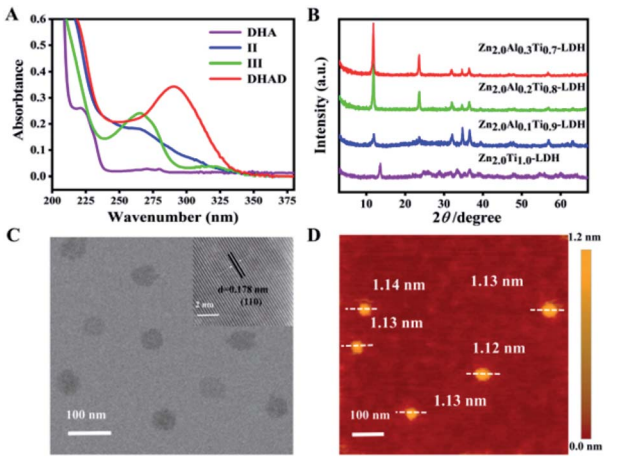

Fig. 1 (A) UV-vis absorption spectra of all compounds. (B) XRD patterns of ZnAlTi-LDH with different ratios and ZnTi-LDH. (C) TEM image of ZnAlTi-LDH. The inset showed the [110] lattice fringe of an LDH phase. (D) AFM image of ZnAlTi-LDH.

(EE) were 146.3% and 73.1% with the mass ratio of DHAD : LDH = 2 : 1 (Fig. 2A). However, the EE quickly decreased to 40.7% when the mass ratio of DHAD : LDH was 4 : 1. As a result, the final DHAD/LDH sample was fabricated with the mass ratio of DHAD : LDH = 2 : 1. The assembly of DHAD and LDH was demonstrated by the FT-IR spectra (Fig. S16†). Bands at 2965 cm^{-1} (stretching vibration of C–C–H) of DHAD are observed in the final sample, along with the $-NO_2$ characteristic vibration absorption peaks of LDH at 1365 cm^{-1}, indicating the combination of DHAD and LDH nanosheets. The optical properties of DHAD/LDH were analyzed by UV-vis absorption spectra (Fig. 2B). Pure DHAD showed no visible absorption but strong absorption in 200–320 nm. Enhanced absorption of the UV region was achieved when DHAD was hybridized with ZnAlTi-LDH. Moreover, absorption thresholds of DHAD, ZnAlTi-LDH and DHAD/LDH were shown in Fig. 2B inset, from which the bandgap of DHAD/LDH was determined to be ~3.55 eV. This value is smaller than that of ZnAlTi-LDH (~3.71 eV) and pure DHAD (~3.91 eV), accounting for a more visible light range for photocatalytic antibacterial activity. In addition, after the assembly of DHAD and LDH, the sheet-like structure of ZnAlTi-LDH was kept, and the thickness increased to ~1.3 nm (Fig. S17†). The ability of DHAD/LDH to produce ROS was further investigated. The intensity of $^1O_2$ and $^{\bullet}OH$ was detected by electron paramagnetic resonance (ESR) with 5,5-dimethyl-1-pyrroline N-oxide (DMPO) and 2,2,6,6-tetramethyl-1-piperidine (TEMP) as spin probes.[22] As showed in Fig. 2C and D, both $^{\bullet}OH$ and $^1O_2$ could be produced by DHAD/LDH under visible light irradiation (400–780 nm), and the intensity of ROS gradually increased as the irradiation time prolonged from 1 to 5 min. In addition, ESR spectra (Fig. S18†) proved that the ROS production efficiency of DHAD/LDH was better than that of nano-TiO_2 (5–10 nm). Thus, DHAD/LDH can be used as an effective photocatalytic antibacterial agent.

To test the bactericidal activity of DHAD/LDH, *E. coli* and *S. aureus* were used as representative strains, and further experiments were carried out under simulated solar light (400–780 nm, 100 mW cm^{-2}). Based on the *in vitro* inhibition experiments of *S. aureus* with different concentrations of DHAD/LDH, the optimal amount of DHAD/LDH is 200 μg mL^{-1} (Fig. S19†). In subsequent experiments, *E. coli* and *S. aureus* were incubated separately with DHAD, ZnAlTi-LDH, DHAD/LDH (final concentration: 0.2 mg mL^{-1}) in PBS, and then exposed to a solar simulator for different time (0, 5, 10, 20 and 40 min). As shown in Fig. 3A and B, the presence of light had little effect on the actual antimicrobial activity of DHAD, and the intrinsic antibacterial efficiency of *E. coli* and *S. aureus* were 51% and 46% respectively. ZnAlTi-LDH had almost no bactericidal effect in the dark environment. However, after 40 min of illumination, the inhibition rate of *E. coli* and *S. aureus* reached 65% and 61% respectively. For DHAD/LDH, the inhibition rate against *E. coli* and *S. aureus* after 40 min of illumination reached 94% and 91% respectively, which was significantly higher than that of DHAD and ZnAlTi-LDH. Photographs of antibacterial results after 40 min irradiation were shown in Fig. S20.† In order to intuitively observe the antibacterial process of DHAD/LDH, fluorescent staining was used to distinguish the live and dead bacteria, which were stained in green and red respectively. As showed in Fig. 3C, bacteria (*S. aureus*) in the control group were alive. After incubating DHAD/LDH for 6 h, some dead bacteria without irradiation were observed. Subsequently, a significant increase in bacterial death was observed following 5–30 min irradiation. To further reveal the antibacterial mechanism, scanning electron microscope (SEM) was used to observe the morphological changes of *S. aureus*. As showed in Fig. 3D, the normal *S. aureus* was spherical and had a smooth surface. After being treated with DHAD/LDH for 5 min irradiation, the cell walls became a little incomplete and wrinkled. Moreover, severe damage and complete wrinkle were observed on the bacterial surface after 30 min irradiation, indicating the excellent antibacterial ability of DHAD/LDH. In addition, the cytotoxicity of DHAD/LDH toward mouse renal epithelial cells was evaluated (Fig. S21†). When the cells were treated with 500 μg mL^{-1} of DHAD/LDH, the cell viability remained above 98% after 12 hours incubation and above 95% after 24 hours incubation, indicating the excellent biocompatibility.

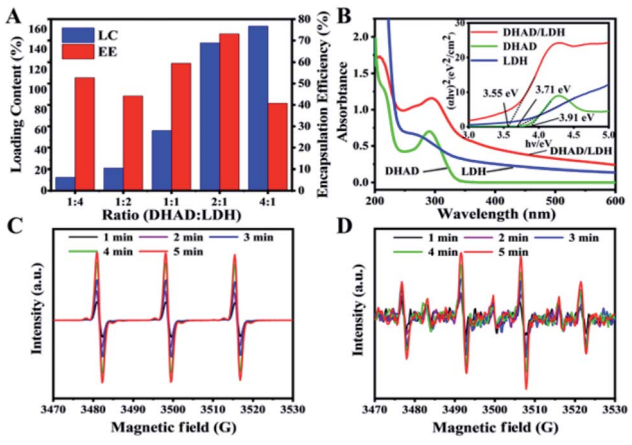

Fig. 2 (A) LC and EE of DHAD with ZnAlTi-LDH at different ratios. (B) UV-vis absorption spectra of DHAD, ZnAlTi-LDH and DHAD/LDH. The inset shows their absorption thresholds. ESR spectra upon irradiation for detection of (C) $^1O_2$, (D) $^{\bullet}OH$ at different times.

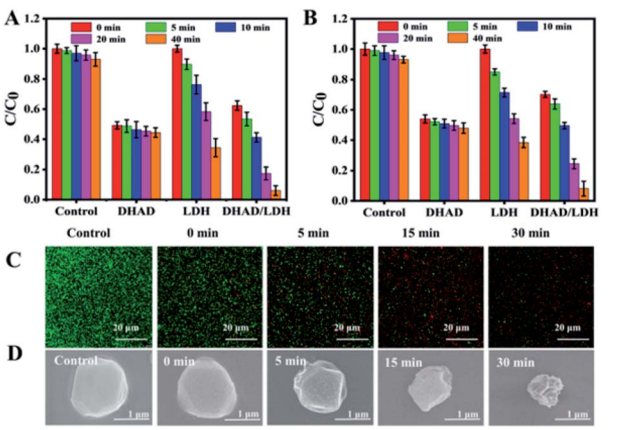

Fig. 3 Antibacterial activity toward *E. coli* (A) and *S. aureus* (B). (C) Relative bacterial fluorescence staining images and (D) SEM images of *S. aureus* treated with DHAD/LDH in different irradiation times.

Subsequently, the skin wound-healing performance of DHAD/LDH was evaluated through wound-infecting mice. As the most common pyogenic cocci, *S. aureus* is an important factor in the cross-infection of the wound. Mice with the wound on the back were infected with *S. aureus* to construct the wound infection model. Later, the wound infected mice were divided into five groups (4 mice per group) and treated with (i) PBS (control), (ii) PBS + light (only light), (iii) DHAD/LDH, (iv) DHAD/LDH + light, (v) commercial anti-inflammatory drugs (mupirocin). As shown in Fig. 4A, due to the antimicrobial activity of DHAD, DHAD/LDH could better promote the wound healing without visible light irradiation than the control group. The wound healing efficiency showed in the group (iv) and group (v) was significantly higher than other groups, and group (iv) showed the quickest reduction of the wound area, indicated the excellent therapeutic effects of the DHAD/LDH with irradiation. As shown in Fig. 4B and S22,† photographs of the control group showed that the wound scabbed slowly when accompanied by inflammation. In contrast, DHAD/LDH with irradiation showed excellent therapeutic effects during the whole wound healing process. Scars appeared on the 4th day, and the wound area was obviously smaller on the 6th day. After 10 days of treatment, the wound was completely healed. Thus, DHAD/LDH could effectively shorten the wound healing time with excellent therapeutic effects.

As mentioned earlier, the new tissue around the wound is extremely fragile and vulnerable to secondary damage from high-energy UV radiation. In consequence, the protective effect of DHAD/LDH against sunburn on mice skin was further evaluated. The depilated mice were divided into four groups and smeared with DHAD/LDH, sunscreen (SPF 30), and PBS on their back respectively. Then the skin was exposed to UVB rays (280–320 nm, 0.1 mW cm^{-2}) two hours per day. The control group without UV irradiation showed no damage. PBS treated skin was significantly damaged by the same UV exposure as showed in Fig. 4C and S23.† The skin of the mice gradually reddened with erythema, and the epidermis became rough gradually. Skin wrinkles appeared later and skin keratinization became serious. Mice treated with sunscreen showed a small amount of erythema while no significant erythema, edema or ulcer was observed in the skin of DHAD/LDH-treated mice after 10 day UV irradiation. Skin tissue slices collected from four groups were stained with hematoxylin and eosin (H&E) (Fig. 4D). In the unprotected group, there was noticeable acanthosis with prominent rete ridges consistent with epidermal hypertrophy. The skin protected by sunscreen was significantly thicker than that of the control group. However, the skin tissue biopsies treated with DHAD/LDH were similar to the control group, demonstrating the excellent UV protection performance of DHAD/LDH composite. Therefore, the results proved that DHAD/LDH-based sunscreen is effective in protecting skin tissue.

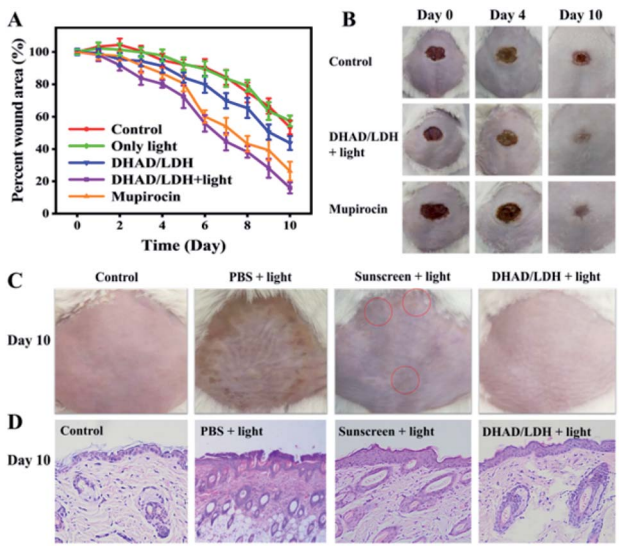

Fig. 4 (A) Percentage wound area treated with different treatment groups for 10 days. (B) Photographs of the treatment process of different treatments on infected wounds. (C) Photographs of UV blocking performance and (D) hematoxylin and eosin stain of the skin slices subjected to different treatments on day 10.

Conclusions

In summary, for the first time, a dual-functional photocatalytic antibacterial and UV resistant composite was fabricated by loading DHAD onto ZnAlTi-LDH nanosheets, possessing excellent UV protection, antibacterial and wound healing performance. ZnAlTi-LDH showed superior loading capacity toward hydrophobic DHAD with an LC of 146.3%. DHAD/LDH composite exhibited prominent $^{\cdot}OH$ and $^{1}O_2$ produced ability under visible light. Combined with the intrinsic antibacterial activity of DHAD and ROS generated ability of ZnAlTi-LDH, DHAD/ZnAlTi-LDH showed a superior antibacterial efficacy toward *E. coli* and *S. aureus* with the bacteria growth inhibition rate of 94% and 91% respectively. Furthermore, bacteria-infected wound experiments indicated that the affected area shrunk and recovered quickly after treated by the composite. Simultaneously, UV exposure experiments showed that DHAD/LDH had excellent UV resistant ability to protect the skin. Considering the advantages of antibacterial activity and UV protection of DHAD/LDH, the potential applications of DHAD/LDH in antibacterial treatment, wound-healing, and UV protection can be anticipated.

Ethical statement

All animal studies were conducted under the guidelines of the National Institute of Health Guiding Principles for the Care and Use of Laboratory Animals, and the overall project protocols were approved by the Ethics Review Committee for Animal Experimentation of the Institute of Clinical Medicine, China-Japan Friendship Hospital, Beijing.

Conflicts of interest

There are no conflicts to declare.

Acknowledgements

This work was supported by the National Natural Science Foundation of China (NSFC: 21521005, 21971007, 21671013, 21601010, 31870556) and the Fundamental Research Funds for the Central Universities (buctylkxj01, XK1806-2, XK1803-05).

Notes and references

1 D. J. Tobin, *Chem. Soc. Rev.*, 2006, **35**, 52–67.
2 L. Wang, X. Zhang, X. Yu, F. Gao, Z. Shen, X. Zhang, S. Ge, J. Liu, Z. Gu and C. Chen, *Adv. Mater.*, 2019, **31**, 1901965.
3 D. Mao, F. Hu, Kenry, S. Ji, W. Wu, D. Ding, D. Kong and B. Liu, *Adv. Mater.*, 2018, **30**, 1706831.
4 J. Qu, X. Zhao, Y. Liang, T. Zhang, P. X. Ma and B. Guo, *Biomaterials*, 2018, **183**, 185–199.
5 Y. Duan, Y. Wang, X. Li, G. Zhang, G. Zhang and J. Hu, *Chem. Sci.*, 2020, **11**, 186–194.
6 A. Gupta, S. Mumtaz, C. H. Li, I. Hussain and V. M. Rotello, *Chem. Soc. Rev.*, 2019, **48**, 415–427.
7 Y. Deng, A. Ediriwickrema, F. Yang, J. Lewis, M. Girardi and W. M. Saltzman, *Nat. Mater.*, 2015, **14**, 1278–1285.
8 L. A. Baker, B. Marchetti, T. N. V. Karsili, V. G. Stavros and M. N. R. Ashfold, *Chem. Soc. Rev.*, 2017, **46**, 3770–3791.
9 S. S. Lucky, K. C. Soo and Y. Zhang, *Chem. Rev.*, 2015, **115**, 1990–2042.
10 C. Mao, Y. Xiang, X. Liu, Z. Cui, X. Yang, K. W. K. Yeung, H. Pan, X. Wang, P. K. Chu and S. Wu, *ACS Nano*, 2017, **11**, 9010–9021.
11 F. Cao, E. Ju, Y. Zhang, Z. Wang, C. Liu, W. Li, Y. Huang, K. Dong, J. Ren and X. Qu, *ACS Nano*, 2017, **11**, 4651–4659.
12 W. Yin, J. Yu, F. Lv, L. Yan, L. R. Zheng, Z. Gu and Y. Zhao, *ACS Nano*, 2016, **10**, 11000–11011.
13 R. Hu, F. Zhou, T. Zhou, J. Shen, Z. Wang, Z. Zhao, A. Qin and B. Z. Tang, *Biomaterials*, 2018, **187**, 47–54.
14 G. Liu, P. Niu, L. Yin and H.-M. Cheng, *J. Am. Chem. Soc.*, 2012, **134**, 9070–9073.
15 G. Fan, F. Li, D. G. Evans and X. Duan, *Chem. Soc. Rev.*, 2014, **43**, 7040–7066.
16 X. Mei, J. Ma, X. Bai, X. Zhang, S. Zhang, R. Liang, M. Wei, D. G. Evans and X. Duan, *Chem. Sci.*, 2018, **9**, 5630–5639.
17 Y. M. Cui, E. Yasutomi, Y. Otani, T. Yoshinaga, K. Ido, K. Sawada and T. Ohwada, *Bioorg. Med. Chem. Lett.*, 2008, **18**, 5201–5205.
18 X. C. Huang, L. Jin, M. Wang, D. Liang, Z. F. Chen, Y. Zhang, Y. M. Pan and H. S. Wang, *Eur. J. Med. Chem.*, 2015, **89**, 370–385.
19 W. M. Zhang, T. Yang, X. Y. Pan, X. L. Liu, H. X. Lin, Z. B. Gao, C. G. Yang and Y. M. Cui, *Eur. J. Med. Chem.*, 2017, **127**, 917–927.
20 Y. M. Cui, E. Yasutomi, Y. Otani, K. Ido, T. Yoshinaga, K. Sawada and T. Ohwada, *Bioorg. Med. Chem.*, 2010, **18**, 8642–8659.
21 L. Peng, X. Mei, J. He, J. Xu, W. Zhang, R. Liang, M. Wei, D. G. Evans and X. Duan, *Adv. Mater.*, 2018, **30**, 1707389.
22 C. Mao, Y. Xiang, X. Liu, Z. Cui, X. Yang, Z. Li, S. Zhu, Y. Zheng, K. W. K. Yeung and S. Wu, *ACS Nano*, 2018, **12**, 1747–1759.

